EPJ Web of Conferences **261**, 02006 (2022) https://doi.org/10.1051/epjconf/202226102006
ANPC 2021

The multi-energetic Au ion implantation of graphene oxide and polymers

Petr Malinsky[1,2,*], *Josef* Novák[1,2], *Eva* Štěpanovská[1,2], *Petr* Slepička[3], *Václav* Švorčík[3], *Kateřina* Szőkölová[4], *Petr* Marvan[4], *Zdeněk* Sofer[4], *Anna* Mackova[1,2]

[1]Nuclear Physics Institute of the Czech Academy of Sciences, v. v. i., 250 68 Rez, Czech Republic
[2]Department of Physics, Faculty of Science, J.E. Purkinje University, Pasteurova 15, 400 96 Usti nad Labem, Czech Republic
[3]Department of Solid State Engineering, University of Chemistry and Technology, 166 28 Prague, Czech Republic
[4]Department of Inorganic Chemistry, University of Chemistry and Technology, 166 28 Prague, Czech Republic

Abstract. The electric properties of polymers are increasingly important in a wide range of applications such as sensors, energy storages, microelectronics, and filtration membranes among others. In this work, the effect of multi-energetic Au ion implantation on the graphene oxide (GO), polyimide (PI), polyethylene terephthalate (PET) and polylactide (PLLA) elemental, chemical, structural end electric properties is presented with potential application in 3D metal-dielectric structure synthetization. The three energies, 3.2, 1.6, 0.8 MeV of Au ions with fluence 3.75×10^{14} cm^{-2} were used in ascending or descending order to create two sample sets, which were subsequently analysed by RBS, ERDA, EDS and AFM. RBS analysis was used for Au-depth profile characterization in the implanted samples, the profiles agree reasonably with those simulated by SRIM code. Electrical properties were investigated by standard two-point technique with respect to the used parameters of the ion irradiation. The sheet resistance decreases after ion irradiation and it is evident that the ascending order of ion implantation energies has more significant effect on the conductivity enhancement compare to the descending one.

1 Introduction

Fast-growing modernization and industrialization has a negative impact on the growth of the pollution in the air. Thus, the gas sensors are indispensable for the environment and human health protection. The electrochemical resistive types of gas sensors are recently the widely used as sensors and the polymers are huge candidates in sensing applications due to its low cost, commercial availability, and easy deposition on different transducers [1]. Moreover, some usable polymers (e.g. PLLA) are biocompatible and biodegradable and can be used for the fabrication of environmentally friendly sensors. And already, the graphene and its derivatives (especially graphene oxide and reduced graphene oxide) have aroused significant interest for ultrasensitive gas detectors due its high carrier mobility, extraordinary surface area, unique sensing performance, room-temperature working conditions and tremendous application prospects [2,3]. Moreover, the sensitivity of

*Corresponding author: malinsky@ujf.cas.cz

graphene or polymer based sensors can be further enhanced via doping by metal or its oxides or functionalization by ion irradiation [4,5]. The ion irradiation is an efficient technique for the chemical and functional property modification that in case of organic compounds provides possibility of resulting properties selection (degree of reduction, sp^2/sp^3 carbon hybridization ratio modification, catalytic and sensory properties, and dielectric properties). The conductive polymers have important repercussions in the field of flexible electronics, and in sensing technology, and plenty studies of ion-implantation into polymers reported an electrical conductivity enhancement due to polymer carbonization [6]. When the ion fluence exceed 1×10^{13} cm^{-2}, the threshold for individual ion tracks overlapping is overcome and π-bonded carbon clusters grow, aggregate and form a network of conjugated carbon bonds; for the ion fluences above 1×10^{17} cm^{-2} the aggregation phenomena induce the formation of amorphous carbon and/or graphite like material from irradiated polymer [6,7]. Thus, in the range between 5×10^{13} cm^{-2} and 1×10^{17} cm^{-2}, the nucleation and growth of nano-sized carbon-enriched clusters is expected to take place until a quasi-continuous carbonaceous buried layer is formed [6]. The electron hopping or tunnelling between the conductive carbon islands is then considered as the origin of the electrical conductivity of irradiated polymers [8]. The decorating and functionalization of graphene or polymer by ion implantation significantly increases its sensory properties [9,10]. The gas sensor morphology also significantly affects the sensing performance [11] and the combination of multi-energy ion implantation with ion microbeam provides the possibility to the preparation of spatially well-defined structures in both vertical and horizontal directions. The vertical structure also makes it possible to control the trans-conductance and sensitivity of the implanted layer by applying an external field. The aim of the present work is to give a further contribution to the understanding in the field of energetic ion beam preparation of spatially well-defined 3D metal-dielectric structures with potential applications in field-effect sensors and micro-electronic devices. The four different dielectric matrixes (PI, PET, PLLA, and GO) were implanted by Au ions with three different energies to create three independent layers of Au/insulator composite in polymer or graphene oxide and also for study of these prepared structures.

2 Experimental

Modified Hummers method was used for GO preparation as it is described in [12]. GO film was prepared by filtration on a polycarbonate membrane. Density of the prepared GO films, 1.36 $g{\cdot}cm^{-2}$, was determined by weighing a precisely cut-out part of the GO film. The 50-μm-thick foils of PI – Kapton, PLLA and PET – Mylar were supplied by Goodfellow, Ltd [13,14]. The prepared GO and polymer foils were implanted by the Au ions gradually with three different energies in the ascending or descending order. By this way two sets of samples were prepared, the first one irradiated by Au ions with energies 3.2, 1.6 and 0.8 MeV and the second one with energies 0.8, 1.6 and 3.2 MeV. The implantation was done in the implantation chamber installed at the 3 MV Tandetron MC 4130 accelerator by the ion current densities in the range 8–15 $nA.cm^{-2}$ and to the ion fluence 3.75×10^{14} cm^{-2}. Thus, each foil was implanted with a total Au-ion fluence 1.125×10^{15} cm^{-2} at various depths. Rutherford Back-Scattering spectrometry (RBS) and Elastic Recoil Detection Analysis (ERDA) were employed for the determination of GO and polymer composition and elemental depth profiling before and after the Au-ion irradiation. RBS spectra were collected using a beam of 2.0 MeV He^+ ions. An Ultra-Ortec PIPS detector recorded He^+ ions backscattered at a laboratory scattering angle of 170° in Cornell geometry. To reduce effects of the sample degradation during the RBS analysis, several particular spectra were measured on different beam spots and the final spectrum was obtained by summing the individual spectra. The ERDA spectra were measured using 2.0 MeV He^+ ions with the

primary beam coming at an angle of 75° with respect to the foil surface normal and with hydrogen atoms recoiled at a scattering angle of 30° registered with the PIPS detector covered by a 12 μm Mylar foil. The typical ion current used during the RBS/ERDA analysis was 5 nA. SIMNRA code [15] was used for RBS spectra evaluation and O, H and Au elemental depth profiling. Energy-Dispersive X-ray Spectroscopy (EDS) was used to get deeper information about the GO and polymer foils elemental modification caused by the Au-ion irradiation. The EDS spectra were measured with the Scanning Electron Microscope (SEM) with a field emission gun electron source (TescanLyra dual beam microscope). For measurements, the samples were pasted onto carbon conductive tape and analysed using a 10 kV electrons. The surface morphology was determined with an Atomic Force Microscope (AFM, Dimension ICON, Bruker Corp.) in the quantitative nanoscale mechanical (QNM) mode on air. SCANASYST-AIR silicon tip on nitride lever with a spring constant of 0.4 $N \cdot m^{-1}$ was used. NanoScope Analysis software was applied for data processing. The characteristics of the electric properties of pristine and irradiated samples were studied by the standard 2-point method utilizing the Keithley 6221 Ultra-sensitive Current Source and Keithley 6517B Electrometer/High Resistance Meter. For the sheet resistance measurement two Au contacts, 50 nm thick and 10 mm long, with relative distance 1 mm were sputtered on the surface of GO and polymer foils.

3 Results and Discussion

Electronic energy stopping power of implanted ions leads to atom ionization, electron excitation, bond disruption and subsequent creation of free radicals [7]. Contrary, the nuclear energy stopping power leads to atom knocking and vacancies production [16]. The electronic stopping in polymers containing heteroatoms leads also to the gaseous low mass fragments release and subsequent to dehydrogenation [17]. We made the initial estimation of the Au-ion energy losses and ranges in GO, PI, PET and PLLA foils by the SRIM code [16], where the calculation was performed using the full cascade MC simulation. The GO initial composition was based on the real sample analysis. The composition and properties of polymers were obtained from the SRIM compound dictionary and from [13,14]. Table 1 displays ratios of nuclear to electronic stopping power (S_n/S_e) and ranges of the Au-ions for all energies. It is clear that the nuclear stopping plays a main role in this case and we can expect a massive bond rupturing, low-mass fragments release deoxygenation and dehydrogenation of the implanted layer. The threshold from which carbonisation occurs in polymers is 150–200 eV/nm [18] and we can predict from SRIM simulation significant increasing of carbon concentration that should lead to the conductivity enhancement. On the Fig. 1, one can see the chosen distributions of the SRIM calculated Au depth profiles of 3.2, 1.6 and 0.8 MeV Au ions in GO and PLLA together with the nuclear and electronic stopping power depth profiles for illustration. The summary of the projected ranges Rp is presented in Table 1. The mean projected range of 3.2 MeV Au ions is ~ 1000 nm, 1.6 MeV Au-ions reach the mean depth higher than 500 nm and 0.8 MeV Au ions most often stop before reaching of 300 nm and is evident that Au would create three well distinguishable layers. The influence of the nuclear stopping power significantly grows with the increasing depth and the Au-ion descending energy.

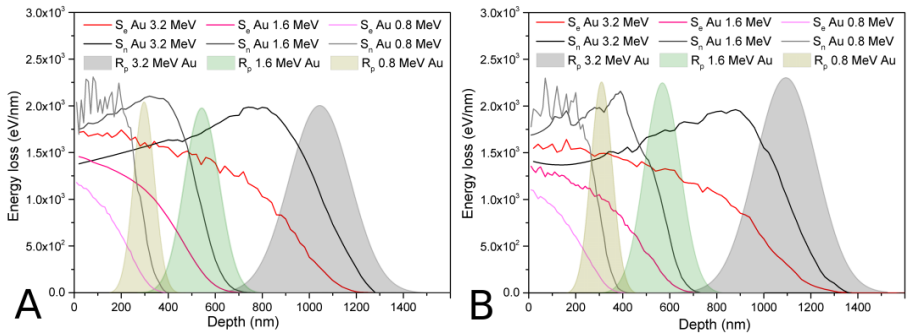

Figure 1. The SRIM calculated Au-depth distribution, nuclear stopping powers (S_n) and electronic (S_e) stopping powers of Au ions with energies 3.2, 1.6 and 0.8 MeV in GO (A) and PLLA (B).

Table 1. The ratios of nuclear and electronic stopping of Au ions and their projected ranges (Rp) with energies 3.2, 1.6 and 0.8 MeV in GO, PLLA, PI and PET matrix.

	Au 3.2 MeV S_n/S_e	Au 1.6 MeV S_n/S_e	Au 0.8 MeV S_n/S_e	Rp (nm) 0.8/1.6/3.2 MeV
GO	1.33	1.85	2.52	297/542/1044
PI	1.32	1.82	2.46	276/502/968
PET	1.42	1.96	2.62	280/514/999
PLLA	1.38	1.95	2.65	309/568/1093

The elemental composition of the pristine and irradiated samples was determined by RBS and ERDA (Fig 2, Table 2). The elemental concentration of C, O and H is presented in the Table 2 and the chosen spectra for GO and PLLA shows the Fig 2 together with the Au-depth profiles. The oxygen release is observable in the implanted GO that is more pronounced for the descending energies (3.2-1.6-0.8 MeV), (Fig. 2A). The PI exhibits the similar behaviour as the GO. The pronounced oxygen release is observable in PLLA only after Au implantation with descending energies (Fig. 2B). The Au implantation with ascending energies (0.8-1.6-3.2 MeV) leads to the O release in PLLA just in the subsurface layer. The behaviour of PET reports such progress as of PLLA. The similar behaviour of the GO and PI versus to the PET and PLLA is connected with the chemical structures. The GO and PI have more aromatic rings in the structure compare to the PET and PLLA. The hydrogen concentration decreases in polymers after Au implantation. This decline is more pronounced after implantation with ascending energies and the most pronounced in PLLA. Contrary, the enrichment of H concentration can be seen in GO, which may be due hydrogenation of the irradiated surface from ambient atmosphere, as observed earlier [19]. The breaking of the volatile compounds and its release leads to the carbonisation, to the accompanying formation of conjugated bonds and conductivity enhancement [18]. The Au depth profiles in GO and PLLA are presented in Figs 2C, D. The position of the Au depth profile in PLLA and in GO implanted with ascending energies well agrees with simulated one by SRIM. The merging of Au profiles in GO implanted with descending energies is connected with the GO high surface roughness and its influence on the RBS analysis. The Au depth profile slight shift to the depth appears in GO, PLLA and PET after implantation with descending energies, which can be connected with sputtering of samples surface layers by 0.8 MeV Au in the last of implantation. It is evident, that the Au creates three well distinguishable independent layers usable in further 3D sensory structures preparation.

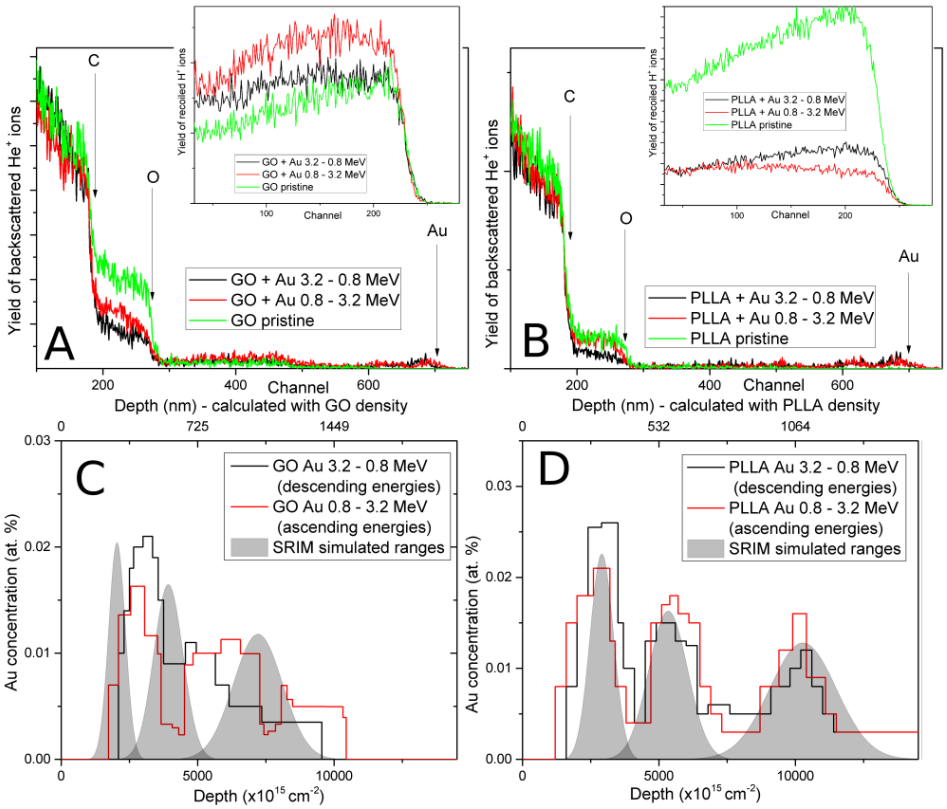

Figure 2. The RBS and ERDA spectra as insets are presented in A, B and detailed Au-depth profiles as-evaluated from RBS with SRIM simulated ranges are presented in(C, D) (inset) of Au ions with energies 3.2, 1.6 and 0.8 MeV in GO and PLLA.

Table 2. The C, O and H concentrations and their ratios on surface (**SU**) and in the depth of ~250 nm (**DE**) in pristine and Au irradiated GO and polymers obtained by RBS and ERDA.

RBS/ ERDA		Pristine					0.8->3.2 MeV ascending energies					3.2->0.8 MeV descending energies				
		C	O	H	C:O	C:H	C	O	H	C:O	C:H	C	O	H	C:O	C:H
GO	**SU**	65.9	21.6	9.8	3.1	6.7	77.6	7.1	11.8	10.9	6.6	78.8	7.1	10.2	11.1	7.7
	DE						71.3	10.4	14.9	6.9	4.8	76.6	7.2	12.5	10.6	6.1
PET	**SU**	53.4	9.3	37.3	5.7	1.4	79.0	4.3	16.6	18.4	4.8	74.0	2.8	23.2	26.4	3.2
	DE						73.3	9.6	17.1	7.6	4.3	73.2	2.8	24.0	26.1	3.1
PLLA	**SU**	53.3	5.3	41.4	10.1	1.3	87.2	3.3	9.6	26.4	9.1	79.5	3.4	17.1	23.4	4.6
	DE						82.2	5.8	12.0	14.1	6.9	79.2	3.3	17.5	24.0	4.6
PI	**SU**	56.4	12.8	25.6	4.4	2.2	71.6	6.9	15.9	10.4	4.5	74.6	3.1	16.8	24.0	4.4
	DE						71.8	7.0	15.6	10.3	4.6	74.9	3.2	16.2	23.4	4.6

The Energy Dispersive Spectroscopy (EDS) provides a qualitative evaluation of the elemental composition changes between the non-irradiated and irradiated parts of the substrates (see Table 3). The accessible information depth of EDS using 10 keV electrons in our samples is approximately 1 μm, which is comparable with that of RBS. RBS is able to provide information from individual depths, while the EDS tells just about the integral amount of elements in the whole analysed depth. The oxygen release and associated carbonization are observed in the EDS after the Au-ion implantation, which is more

pronounced for the samples implanted with descending energies. This finding is in agreement with above described RBS results.

Table 3. The C, O concentrations and their ratios in pristine and Au irradiated GO and polymers obtained by EDS.

EDS	Pristine			0.8->3.2 MeV ascending energies			3.2->0.8 MeV descending energies		
	C	O	C:O	C	O	C:O	C	O	C:O
GO	65.6	34.1	1.9	84.1	15.3	5.5	86.1	13.2	6.5
PET	71.9	28.1	2.6	85.3	14.7	5.8	92.9	7.1	13.1
PLLA	61.9	38.0	1.6	88.7	11.2	7.9	95.2	4.6	20.7
PI	82.0	18.0	4.6	85.1	12.4	6.9	90.0	6.3	14.3

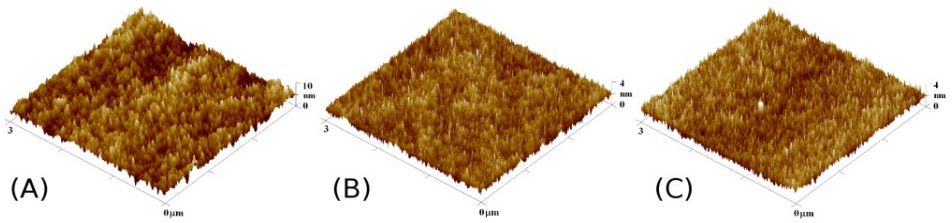

Figure 3. The 3D AFM image of surface of pristine PI (A), PI irradiated by Au ions with ascending energies (B) and PI irradiated by Au ions with ascending energies (C).

The surface morphology changes, as studied by AFM, are introduced in Table 3, where the roughness parameters are presented for all samples and in the Fig 3, where the 3D surface of chosen PI is shown for ilustration. The pristine GO surface exhibits the morphology with obvious irregularities and significant roughness, which increases even more after implantation. The roughness increasing is more pronounced for GO implanted by Au ions with descending energies, which can be connected with the GO surface sputtering with the last Au-ion implantation with lowest energy 0.8 MeV, as also precluded from RBS. As a result of the ion implantation, the roughness also dramatically increase on the surface of PET and the only mild roughness increasing has been observed on the PLLA surface. Rather different situation is observed for the PI, where the Au-ion implantation leads to the polymer rougness decreasing. The ion irradiation leads to the surface roughness change of polymes based on their chemical structure. PI as a polymer with complex monomer shows the surface smoothening under the ion irradiation. Contrary, in the polymers with simpler structure (PET, PLLA) can the chain scission leads to surface roughness increasing [20].

Table 4. The surface roughness arithmetic average height parameters (R_a) and the mean roughness parameters (RMS) of pristine and modified samples as obtained by AFM.

AFM	Pristine		0.8->3.2 MeV ascending		3.2->0.8 MeV descending	
	R_a	RMS	R_a	RMS	R_a	RMS
GO	49.2	61.6	65.6	79.8	99.6	126
PET	0.46	0.62	0.64	0.79	0.67	0.88
PLLA	6.5	7.3	8.3	10.4	6.9	8.5
PI	2.33	3.45	0.32	0.43	0.53	0.72

The Au-ion implanted samples sheet resistances, displayed in Figure 4, were measured to get information about the changes in electrical properties. The conductivity of all samples increases after the Au implantation in comparison with that of pristine. In the PET, GO and PLLA the conductivity increase is more pronounced for samples implanted with Au-ions ascending energies. The changes in the electrical conductivity after implantation can be attributed to the carbonization of thin subsurface layer, as proved by ERDA/RBS measurements and predicted by SRIM, and to the subsequently growth of the carbon clusters, which form a conjugated network. A conductive network with many cross-linked carbon connections then facilitates charge carrier transfer in the modified surface. The conductivity enhancement in polymers after the change of energies sequence is related to the higher concentration of carbon on the surface and the hydrogen concentration decrease, and is more pronounced in PPLA and PET with ascending energies and in PI with descending energies. Contrary, the conductivity of the GO after implantation with ascending energies is better in spite of lower carbon concentrationin the surface. This trend can be connected with GO porousity and islet structure, which can caused higher influence of the deeper layers, where the carbon concentration is higher.

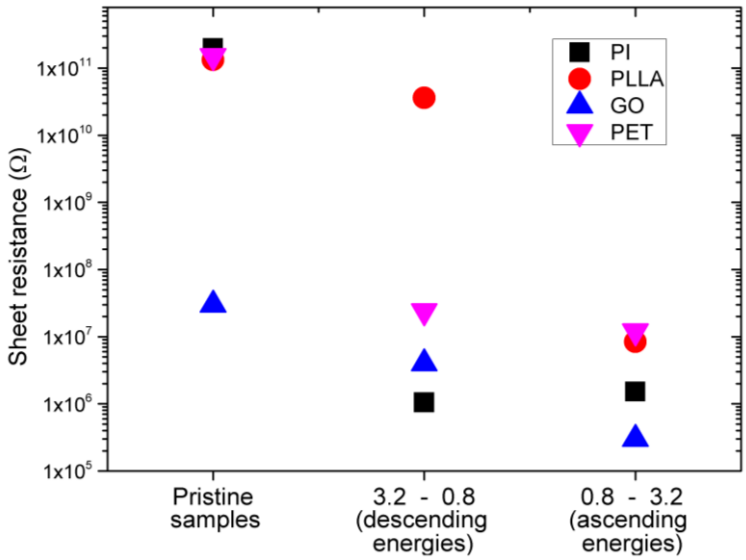

Figure 4. The electric resistance of GO, PLLA, PI and PET before and after Au ion irradiation.

4 Conclusion

In this work, the 3D Au-dielectric structures were synthetized by ion implantation in PI, PET, PLLA and GO with potential applications in the field-effect micro-sensory and micro-electronic application. We proved, that the conductive multilayer system with Au-doped and un-doped parts can be created in dielectric samples by ion implantation. The best quality of Au distribution was found in PLLA with three well separated layers. We can say that the Au-ion implantation with descending energies has more significant influence on the oxygen composition, while the ascending energies order influence little bit more the hydrogen concentration in polymers. The electric conductivity enhancement in polymers is connected with carbonization of the surface layer, caused be decreasing of both, oxygen as well as hydrogen concentration. It seems that Au implantation starting with higher energy causes more damage. The descending Au-ion energies being implanted mean, that as a first

the deeper layer is irradiated, and then the next sub-sequent Au-ion implantations are provided into the modified layer and may cause more damage. Opposite situation is in case of the ascending energy implantation, where in the first step the surface is significantly modified by the Au-ions with the lowest energy of 0.8 MeV and this partially carbonized layer with gold particles inside can than play a function of sample protection.

The research has been carried out at the CANAM (Centre of Accelerators and Nuclear Analytical Methods) infrastructure LM 2015056 and promoted by the Czech Science Foundation (GACR No. 19-02482S) and University of J.E. Purkyne project UJEP-SGS-2021-53-005-2. This publication was supported by OP RDE, MEYS, Czech Republic under the project CANAM OP, CZ.02.1.01/0.0/0.0/16_013/0001812.

References

1. J. Boudaden, M. Steinmaß, H.E. Endres, A. Drost, I. Eisele, Ch. Kutter, P. Müller-Buschbaum, Sensors **18**, 1516, (2018)
2. D. Zhang, J. Tong, B. Xia, Q. Xue, Sensors and Actuators B **203**, 263–270, (2014)
3. T. Wang, D. Huang, Z. Yang, S. Xu, G. He, X. Li, N. Hu, G. Yin, D. He, L. Zhang, Nano-Micro Lett. **8**, 95–119, (2016)
4. N.M. Nurazzi, N. Abdullah, S.Z.N. Demon, N.A. Halim, A.F.M. Azmi, V.F. Knight, I.S. Mohamad, Nanotechnology reviews **10**, 330-369, (2021)
5. F.A.A. Nugroho, I. Darmadi, L. Cusinato, A. Susarrey-Arce, H. Schreuders, L.J. Bannenberg, A.B. da Silva Fanta, S. Kadkhodazadeh, J.B. Wagner, T.J. Antosiewicz, Anders Hellman, V.P. Zhdanov, B. Dam, Ch. Langhammer, Nature materials 18, 489-495, (2019)
6. V. Resta, G. Quarta, I. Farella, L. Maruccio, A. Cola, L. Calcagnile, Nucl Instrum Meth B **331**, 168-171, (2014)
7. V. Popok ,Rev Adv Mater Sci.30, 1-26, (2012)
8. M. Döbeli , T.J. Jones , A. Lee , R.P. Livi,T.A. Tombrello, Radiation Effects and Defects in Solids **118**, 325-339, (1991)
9. R. Kumar, D.K. Avasthi, A Kaur, Sensors and Actuators B **242**, 461-468, (2017)
10. C.R. Minitha, L.R. Nivedita, K. Asokan, R.T.R. Kumar, Nucl Instrum Meth B **450**, 257-261, (2019)
11. A. Mirzaei, J.H. Lee, S.M. Majhi, M. Weber, M. Bechelany, H.W. Kim, S.S. Kim, J. Appl. Phys.**126**, 241102, (2019)
12. O. Jankovský, P. Šimek, J. Luxa, D. Sedmidubský, I. Tomandl, A. Macková, R. Mikšová, P. Malinský, M. Pumera, Z. Sofer, Chem Plus Chem **80**, 1399–1407, (2015)
13. http://www.goodfellow.com
14. W. Martienssen, H. Warlimont, Springer Handbook of Condensed Matter and Materials Data, Springer-Verlag, Berlin, Heidelberg, 2005, 978-3-540-30437-1.
15. M. Mayer, SIMNRA version 6.06, Max-Planck-Institut fur Plasmaphysik Garching, Germany, 2006 Available at: http://www.rzg.mpg.de/~mam/
16. J.F. Ziegler, Nucl Instrum Meth B. **219–220**, 1027-1036, (2004)
17. D.V. Sviridov, Russ Chem Rev. **71**, 315–327, (2002)
18. V.N. Popok, I.I. Zarko, R.I. Khaibullin, A.L. Stepanov, V. Hnatowicz, A. Mackova, S.V. Prasalovich, Appl. Phys. A **78**, 1067–1072, (2004)

19. P. Malinský, M. Cutroneo, A. Macková, V. Hnatowicz, M. Florianová, M. Boháčová, D. Bouša, Z. Sofer, Surface and Coatings Technology **342**, 220–225, (2018)
20. R. Mikšová, A. Macková, M. Cutroneo, P. Slepička, J. Matoušek, Surface and Interface analysis **48**, 566-569, (2016)